Transit of Mercury May 9 12:00-15:00

Telescopes in the University Parks by the Keble Gate

Mercury crosses the disk of the sun – giving an idea of exoplanet transit search requirements.

Mercury's radius is 2440km (~40% of Earth's)

Diagnostics of electron density and temperature in Nebulae

- Different processes dominate under different conditions, and so in order to know which approach to take, we need to be able to estimate the prevailing density and temperature in the medium under study.

- We can do this by using pairs of transitions that are sensitive to the density, e.g. because they have very different collisional rates, and so the ratio of the line intensities varies as a function of the density or temperature.

- Most diagnostic measurements use lines in the optical because they are well proven and are well understood, but as instruments in other wavelength regimes have become more sensitive, diagnostics in e.g. the infrared are becoming more important, and benefit from reduced sensitivity to the effects of interstellar reddening

Electron Temperature

The electron temperature reflects the balance between the heating rate of the gas via photo-ionization and the cooling of the gas by the emission of photons that escape the nebula.

The cooling rate increases rapidly with temperature (collisions become more likely).
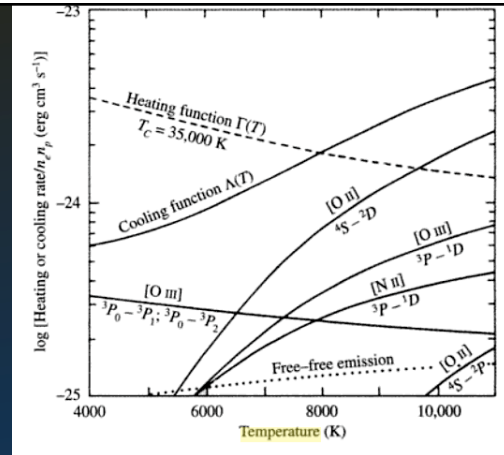
The heating rate decreases slowly as the temperature increases because:

– the recombination rate decreases with temperature
– collisional ionizations decrease the fraction of neutral hydrogen, reducing κ_ν

This thermostatic process gives most HII regions temperatures around 10^4 K.

In the figure (from Kwok), the heating rate represents that of a 35,000 K star, and the total cooling rate, together with the major contributions from [O II], [O III] and [N II] lines is shown together with the free-free continuum. The resulting electron temperature, 8000 K, is given by the intersection of the heating and cooling curves.

Temperature

Higher ionization reduces the O II fraction, decreasing the cooling rate.

Lower heavy element abundances decrease the cooling efficiency of collisionally excited lines, and so lead to higher electron temperatures.

Dust depletes heavy elements from the gas and so also reduces line cooling

High densities gives rise to collisional de-excitation of some excited levels and can also reduce line cooling

Diagnostics of Density and Temperature in ionized nebulae

Measurements of T_e:

We consider the ratio of two lines that are sensitive to the electron temperature to get an estimate of T_e.

We therefore consider a 3 level atom, where the upper two levels are populated by collisions, which then decay radiatively to the same lower level.

For typical nebula conditions, the induced transitions can be neglected, and so we consider only the collisional and radiative transitions.

At very low densities, the upper levels are populated via collisional excitation from the ground state and decay via spontaneous emission

Electron Temperature

- Ideal configurations for these measurements include O III and N II. In O III, the $^1S_0$ and $^1D_2$ excited states are separated by about the same energy (2.8 and 2.5eV) and produce transitions in the middle of the visible spectrum. Note that these violate the $\Delta\ell = \pm1$ selection rule for electric dipole transitions

- The level intervals are such that the lines are quite close in wavelength, so that differential extinction effects are not too great.

- All possible transitions are shown in this diagram, but we will consider a simplified 3 level atom .

- Note that IR fine structure lines can be employed for density estimates.

- At low densities, every collisional excitation results in emission of a photon, so only collisions from the ground state are considered
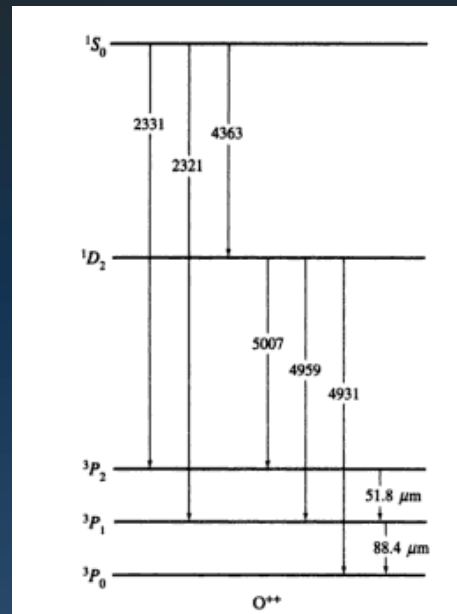
O III Energy Levels

Equations of statistical equilibrium give:

$N_2 A_{21} = N_1 C_{12} n_e + N_3 A_{32}$ and $N_3 (A_{31} + A_{32}) = N_1 C_{13} n_e$

The flux ratio of the (3-2) to (2-1) lines is

$$\frac{F_{32}}{F_{21}} = \frac{h\nu_{32} A_{32} N_3}{h\nu_{21} A_{21} N_2}$$

Substituting for N_3 and N_2:

And with

$N_3 = N_1 n_e C_{13} / (A_{31} + A_{32})$

$$\frac{F_{32}}{F_{21}} = \frac{h\nu_{32}[N_1 n_e C_{13} - N_3 A_{31}]}{h\nu_{21}[N_1 n_e C_{12} + N_3 A_{32}]}$$

$$\frac{F_{32}}{F_{21}} = \frac{\nu_{32}[A_{32} C_{13}]}{\nu_{21}[(A_{32} + A_{31})C_{12} + C_{13} A_{32}]}$$

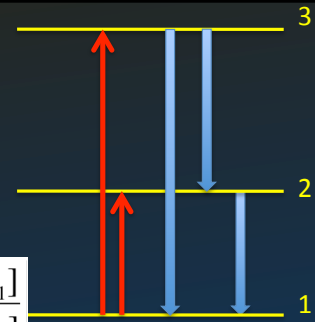In practice,

$C_{13} A_{32} \ll C_{12} (A_{31} + A_{32})$

$$\frac{F_{32}}{F_{21}} = \frac{\nu_{32}[A_{32} C_{13}]}{\nu_{21}(A_{32} + A_{31})C_{12}}$$

Recall that

$$C_{12} = 8.6 \times 10^{-12} \frac{\overline{\Omega}_{12}}{g_1} T_e^{-1/2} e^{-\chi_{12}/kT_e}$$

So substituting for the ratio of C_{13}/C_{12} gives:

$$\frac{F_{32}}{F_{21}} = \frac{\nu_{32}}{\nu_{21}} \frac{A_{32}}{(A_{31} + A_{32})} \frac{\overline{\Omega}_{13}}{\overline{\Omega}_{12}} e^{-E_{32}/kT_e}$$

Measurements of electron temperature

$$\frac{I(4363A)}{I(4959 + 5007A)} = \frac{\nu_{32}}{\nu_{21}} \frac{A_{32}}{(A_{31} + A_{32})} \frac{\overline{\Omega}_{13}}{\overline{\Omega}_{12}} e^{-E_{32}/kT_e}$$
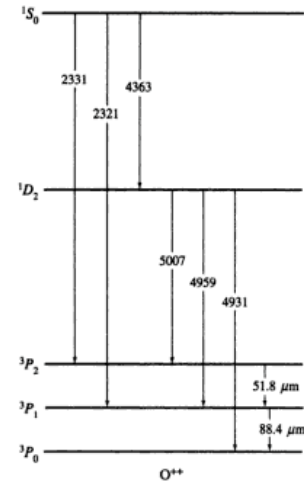
For OIII, we have two closely spaced lines from 2-> 1, and we can express this in terms of the 3 lines measured. This expression depends only on known or calculable quantities: wavelength, A values, collision strengths and the temperature.

Measurement of the line ratio can be used to infer the temperature of the emitting gas, provided that the lines come from the same volume and that the electron density is <n_{crit} (which is >10^{12}m-3 for the 2-1 transition).

O III as a temperature diagnostic

$$\frac{I(4363A)}{I(4959+5007A)} = \frac{\nu_{32}}{\nu_{21}} \frac{A_{32}}{(A_{31}+A_{32})} \frac{\overline{\Omega}_{13}}{\overline{\overline{\Omega}}_{12}} e^{-E_{32}/kT_e}$$

Transition	Ω	A	$N_e^*(m^{-3})\,at\,10^4\,K$	
$^3P_2-^1D_2$ }		0.021	{	λ5007
$^3P_1-^1D_2$ }	2.4	7.1×10^{-3}	{ 7×10^{11}	λ4959
$^3P_0-^1D_2$ }		1.9×10^{-6}	{	
$^3P_2-^1S_0$ }		7.1×10^{-4}	{	
$^3P_1-^1S_0$ }	0.34	0.23	{ 3×10^{13}	
$^1D_2-^1S_0$	0.31	1.6	3×10^{13}	λ4363

O III as a temperature diagnostic

$$\frac{I(4363A)}{I(4959+5007A)} = \frac{\nu_{32}}{\nu_{21}} \frac{A_{32}}{(A_{31}+A_{32})} \frac{\overline{\Omega}_{13}}{\overline{\overline{\Omega}}_{12}} e^{-E_{32}/kT_e}$$

For OIII
1st term ~ λ 4990/4363   = 1.14
2nd term ~ 1.6/(0.23+1.6)   = 0.87
3rd term ~ 0.34/2.4   = 0.14

$$\frac{I(4363A)}{I(4959+5007A)} = 0.14 \; e^{-33000/T_e}$$

[OIII] Line Ratio dependence on T_e

5000   10,000   20,000

Temperature (K)

10^1

10^0

10^{-1}

$\dfrac{I(4363)}{I(5007 +4959)}$

10^{-2}

10^{-3}

10^{-4}

10^3 10^4 10^5
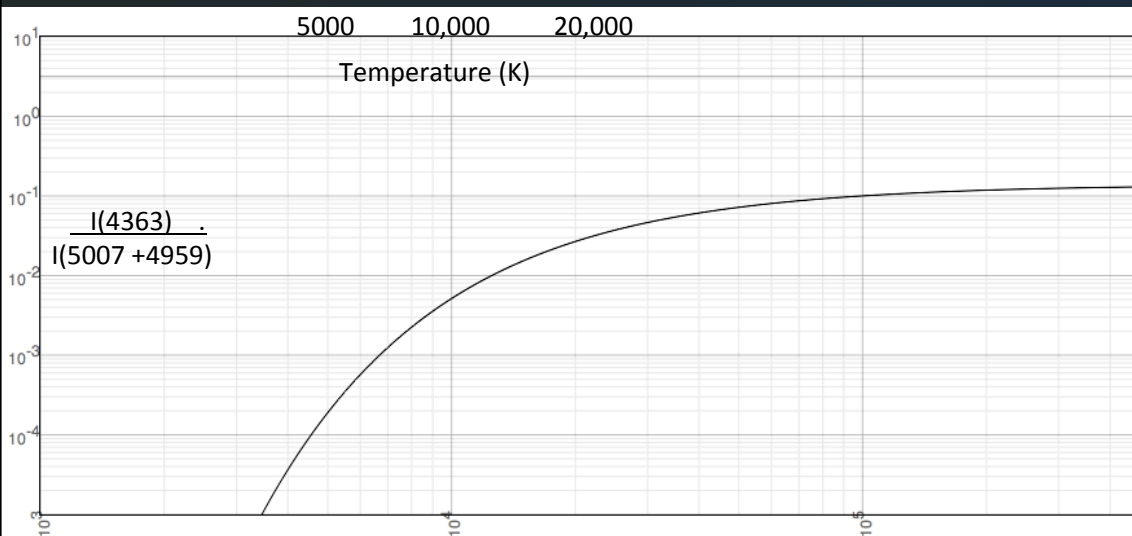
Maximum sensitivity in the region 5000 < T < 20,000 K, varying by a factor ~ 100 – ideal for typical nebular condition

But note that Intensity of λ4363 drops rapidly with decreasing T_e

and that this diagnostic is valid where the density << the critical density

---

Temperature estimates from [N II]

N II shares the same electronic structure as O III, so the lines at 5755, 6548 and 6583Å can be used to estimate T_e in the same manner.
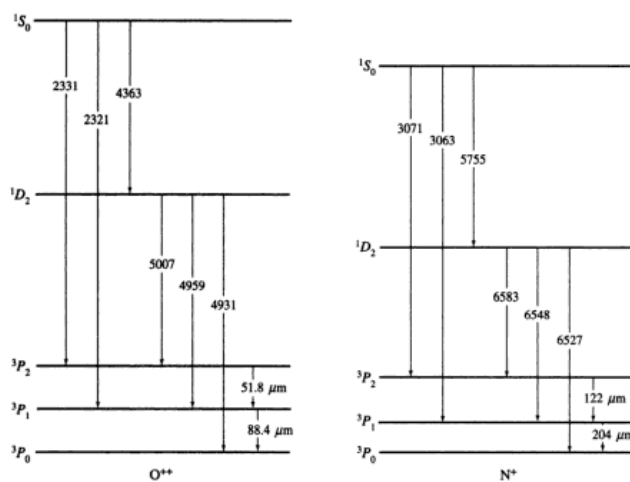
In this case, the equation reduces to:

Figure 5.23
The ground-state multiplet of O^{++} and N$^+$. The magnetic dipole $^1D_2 - {}^3P_{1,2}$ transitions of [O III] at λ4959 and λ5007 Å are among the brightest forbidden lines in the ISM. Also shown are the infrared fine-structure lines in ^3P (Section 5.3).

$$\frac{I(5755A)}{I(6548+6583A)} = 0.13 \; e^{-25000/T_e}$$

The electron temperature in nebulae

With a homogenous nebula, estimates of T_e from different lines should give the same result.

However, the [O III] lines (35-55 eV) sample a higher excitation region on average than the [N II] lines (14-30eV), and so are likely to apply to a different physical region.

Multiple diagnostics help to give a more complete picture of nebular conditions (e.g. [Ne V] whose lines are in the UV would represent a high excitation region).
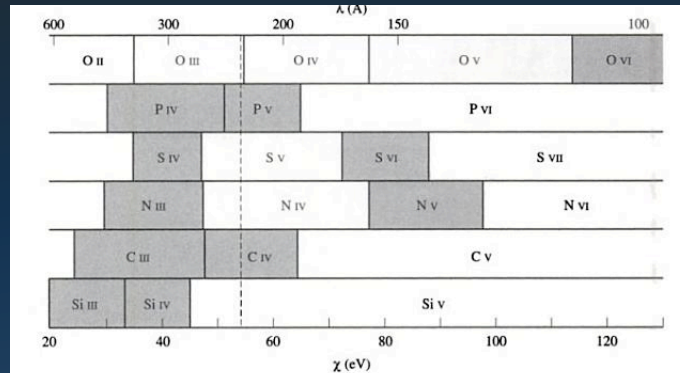

Figure 5.4
Ionization stages as a function of ionization potential for abundant elements (C, N, O, Si, S, and P). Stages with resonance lines in the UV and far UV observable by *HST* and *FUSE* are shaded. The dashed vertical line indicates the ionization potential of He II of 54.4 eV. Ions to the right of this line are likely to be ionized collisionally by high-temperature gas in the ISM (adapted from Massa *et al.* 2003, *ApJ*, **586**, 996).

Density Diagnostics

To estimate the density, we again consider a 3-level atom. Here we want a configuration where the transition from level 3 →1 is a permitted electric dipole transition with a large A value, and the transition from 2 →1 has a much smaller A value, e.g. from a spin-forbidden transition.

While collisional de-excitation is not important for level 3, it may be important for level 2.

In Statistical equilibrium: $N_3 A_{31} = N_1 C_{13} n_e$

And: $N_2 (A_{21} + C_{21} n_e) = N_1 C_{12} n_e$

with $F_{31} = h\nu_{31} N_3 A_{31}$
and $F_{21} = h\nu_{21} N_2 A_{21}$

For the flux ratio of the two lines, We get

$$\frac{F_{31}}{F_{21}} = \frac{\lambda_{21}}{\lambda_{31}} \frac{C_{13}}{C_{12}} \frac{(A_{21} + C_{21} n_e)}{A_{21}}$$

C++ Density Diagnostics

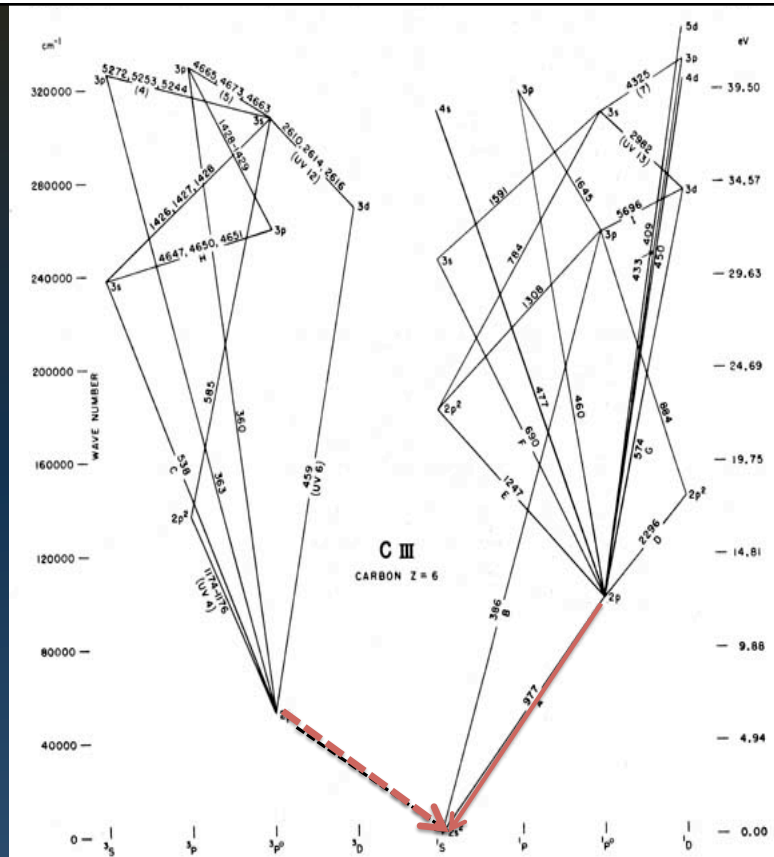CIII has UV transitions between levels :

$2s2p\ ^1P_1$

$2s2p\ ^3P_1$

and

$2s^2\ ^1S_0$

where

$A(^1P_1 - ^1S_0) \sim 2.\ 10^9\ s^{-1}$
at $102352\ cm^{-1}$

$A(^3P_1 - ^1S_0)\ \sim 10^2\ s^{-1}$
at $52367\ cm^{-1}$

which can be used as density estimators

Density Diagnostics

We consider 4 regimes for density estimation:

1. Low Densities: Where $C_{21}\ n_e\ <<\ A_{21}$
and so the flux ratio involves only the collisional excitation rates as in the Coronal Approximation, and is independent of n_e and the A-values. In this regime, there is no dependence upon density.

2. High densities: where $C_{21}\ n_e\ >>\ A_{21}$, but $A_{31} >> C_{31}\ n_e$

then

$$\frac{F_{31}}{F_{21}} = \frac{\lambda_{21}}{\lambda_{31}} \frac{C_{13}}{C_{12}} \frac{(A_{21} + C_{21}n_e)}{A_{21}}$$

simplifies to:

$$\frac{F_{31}}{F_{21}} = \frac{\lambda_{21}}{\lambda_{31}} \frac{C_{13}}{C_{12}} \frac{C_{21}n_e}{A_{21}}$$

Collisional de-excitation is important from level 2, but not from level 3. i.e. where $C_{21} n_e \gg A_{21}$, but $A_{31} \gg C_{31} n_e$

At High densities:

$$\frac{F_{31}}{F_{21}} = \frac{\lambda_{21}}{\lambda_{31}} \frac{C_{13}}{C_{12}} \frac{C_{21} n_e}{A_{21}}$$

but recall that

$$C_{21} = C_{12} \frac{g_1}{g_2} e^{\chi_{12}/kT}$$

so

$$\frac{F_{31}}{F_{21}} = \frac{\lambda_{21}}{\lambda_{31}} \frac{C_{13}}{A_{21}} \frac{g_1}{g_2} n_e \, e^{\chi_{12}/kT_e}$$

The line ratio depends linearly on n_e, and only slowly on Te, provided that χ_{12}/kT_e is small.

However, at high densities F_{21} becomes very small and the weak line becomes difficult to measure, restricting the usefulness.

---

3. Very High Densities: $C_{21} n_e \gg A_{21}$, and $C_{31} n_e \gg A_{31}$

This regime only applies to very dense regions such as in stellar interiors, for permitted transitions (high A-values) and is not useful for nebulae and astrophysical plasmas. It can be relevant where both transitions 3 →1 and 2 →1 have small A-values and are forbidden lines.

Now in Statistical equilibrium: $N_3 (A_{31} + C_{31} n_e) = N_1 C_{13} n_e$
$N_2 (A_{21} + C_{21} n_e) = N_1 C_{12} n_e$

but the collisional terms dominate the spontaneous terms:

With $F_{31} = h\nu_{31} N_3 A_{31}$
And $F_{21} = h\nu_{21} N_2 A_{21}$

$$\frac{F_{31}}{F_{21}} = \frac{\lambda_{21}}{\lambda_{31}} \frac{A_{31}}{A_{21}} \frac{C_{13}}{C_{12}} \frac{C_{21}}{C_{31}}$$

For the intensity ratio of the two lines, we get :

$$\frac{F_{31}}{F_{21}} = \frac{\lambda_{21}}{\lambda_{31}} \frac{A_{31}}{A_{21}} \frac{g_3}{g_2} e^{-(\chi_{13}-\chi_{12})/kT_e}$$

The line ratio is independent of n_e and the level populations are given by the Boltzmann distribution because collisional excitations are balanced by collisional de-excitations.

4. Intermediate Densities: $C_{21} N_e \sim A_{21}$

In this regime, the density is close to the critical density and both the A and C terms contribute to the line intensities.

$$\frac{F_{31}}{F_{21}} = \frac{\lambda_{21}}{\lambda_{31}} \frac{C_{13}}{C_{12}} \frac{(A_{21} + C_{21}n_e)}{A_{21}}$$

The line ratio increases slowly at low densities then increases rapidly as the critical density is approached, before flattening out at high densities. Different lines have different coefficients and so different values of n_{crit}, so again they are sensitive to different densities.

This regime is the most useful for diagnostic purposes.

If collisional excitation is the only process populating the excited level but both collisions and radiative transitions depopulate the excited level, then the absolute flux in a forbidden (or intersystem) line is :

$$F_{21} = \frac{hc}{\lambda_{21}} \frac{0.8}{2} \frac{n_E}{n_H} \int_s \frac{N_1}{n_{ion}} \frac{n_{ion}}{n_E} \frac{C_{12}n_e^2 A_{21}}{(A_{21} + C_{21}n_e)} ds$$

At low densities, $C_{21} n_e \ll A_{21}$ and F_{21} is $\alpha\, n_e^2$ ds and at high densities F_{21} is $\alpha\, n_e$ ds, but the absolute flux increases as n_e increases.
n_E, n_H and n_{ion} are the number densities of the element, hydrogen and ionic state.


As mentioned above, this approach is used for lines of C III.

It can also be used on ions in its isoelectronic sequence: N IV, O V and Si III

This same technique can be employed for pairs of forbidden lines, provided that the A-values of the transitions are significantly different, and in fact such line pairs provide the most commonly used diagnostics.

Commonly used transitions are the doublets of [O II] and [S II] which lie in the ultraviolet and red spectral regions respectively

Here we consider the [O II] lines at 3726 and 3728 Å, which is a very closely spaced doublet and so can only be used for objects where the components are well separated – i.e. where velocity broadening is < 100 km s^{-1}.
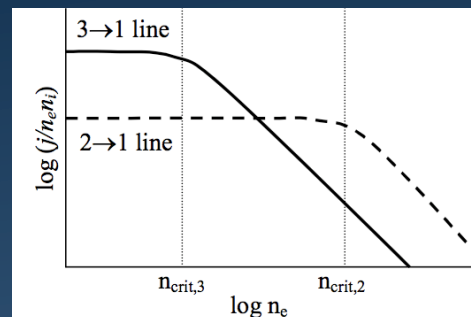
[O II] as a density diagnostic

The [O II] lines at 3726 and 3728Å are transitions within the ground state.

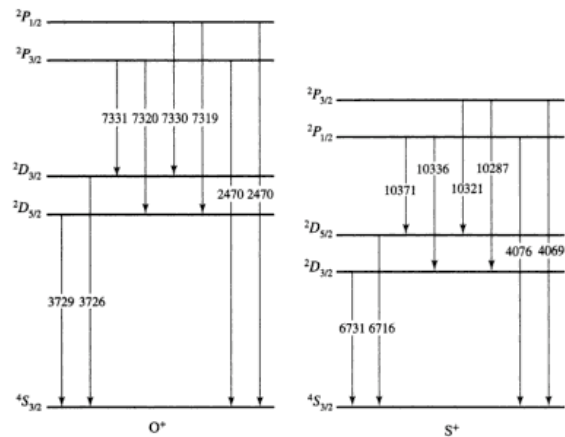They arise from two closely separated fine-structure levels to the singlet ground level.

Figure 5.7
Examples of forbidden transitions within the ground-state multiplet of the ions O^+ and S^+; both are in the p^3 electron configuration. Each transition is labelled with its wavelength in Å.

The transitions are:

	A(s^{-1})	Ω	n_{crit} (m^{-3}) at 10^4 K
$^4S_{3/2} - {}^2D_{3/2}$	1.7×10^{-4}	0.58	1.4×10^{10}
$^4S_{3/2} - {}^2D_{5/2}$	4.8×10^{-5}	0.86	4×10^9

The flux ratio of the [O II] doublet lines is:

$$\frac{F_{31}}{F_{21}} = \frac{\lambda_{21}}{\lambda_{31}} \frac{N_3 A_{31}}{N_2 A_{21}}$$

And the equilibrium equations are :

$$N_3 (A_{31} + C_{31} n_e) = N_1 C_{13} n_e$$
$$N_2 (A_{21} + C_{21} n_e) = N_1 C_{12} n_e$$

Giving:

$$\frac{F_{31}}{F_{21}} = \frac{\lambda_{21}}{\lambda_{31}} \frac{A_{31}}{A_{21}} \frac{C_{13}}{C_{12}} \frac{(A_{21} + C_{21} n_e)}{(A_{31} + C_{31} n_e)}$$

As the two wavelengths differ by only 2Å, the exponential term $\Delta E/kTe$ is very close to unity, and there is almost no dependence on T_e.

But as A_{31} is very different from A_{21}, the flux ratio can be used to measure n_e.

In the high density limit, $n_e \gg n_{crit}$ and this expression becomes

$$\frac{F_{31}}{F_{21}} \approx \frac{A_{31}}{A_{21}} \frac{g_3}{g_2} \approx 2.5$$
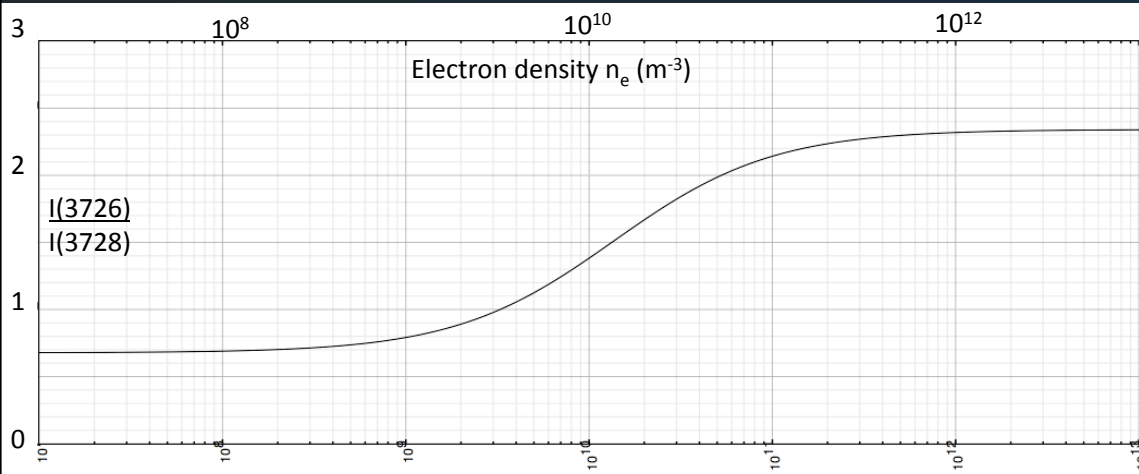
as $\lambda_{21} \approx \lambda_{31}$ and so the ratio depends upon the A values

And in the low density limit, the expression is:

$$\frac{F_{31}}{F_{21}} \approx \frac{C_{13}}{C_{12}} \approx \frac{\Omega_{13}}{\Omega_{12}} \approx 0.66$$

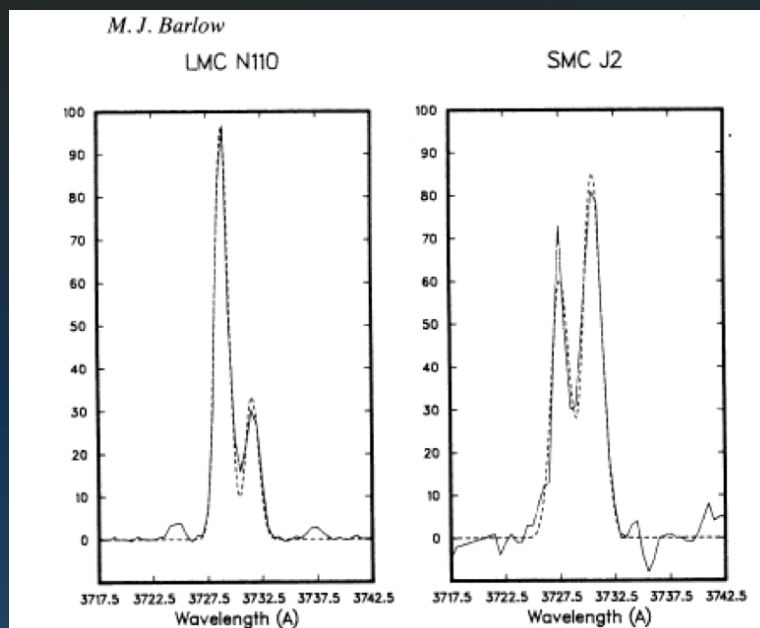Where the ratio depends only on the collision strengths.

[O II] doublet ratio as a function of density

F_{31}/F_{21} for [O II] as a function of N_e at T= 10^4 K, varying from 0.66 at low density to 2.5 in the high density limit.

Maximum sensitivity is near 10^9 - 10^{11} m^{-3}, well matched to many photoionized nebulae

[O II] emission lines in Planetary Nebulae

The [O II] doublets in two PN. LMC N110 has a line ratio 3726/3728 = 2.6 indicating it is near the high density limit, whilst SMC J2 has a line ratio = 0.68 indicating that it is near the low-density limit.

Table 2. Line ratios and electron densities derived using the default atomic parameters described in Table 3.

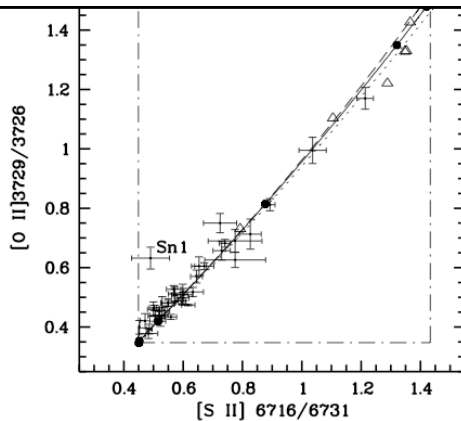| Source[a]	[O II] $\lambda3729/\lambda3726$	$\log N_e$ (cm^{-3})	[S II] $\lambda6716/\lambda6731$	$\log N_e$ (cm^{-3})	[Cl III] $\lambda5517/\lambda5537$	$\log N_e$ (cm^{-3})	[Ar IV] $\lambda4711/\lambda4740$	$\log N_e$ (cm^{-3})
BoBn1							$1.712 \pm .422$	<1.26
Cn 1-5^s			$0.585 \pm .010$	$3.68^{+.03}_{-.03}$	$0.826 \pm .041$	$3.53^{+.05}_{-.06}$	$1.159 \pm .106$	$3.15^{+.20}_{-.36}$
Cn 2-1	$.480 \pm .010$	$3.71^{+.04}_{-.04}$	$0.549 \pm .021$	$3.81^{+.10}_{-.09}$	$0.602 \pm .069$	$3.87^{+.10}_{-.12}$	$0.472 \pm .016$	$4.23^{+.03}_{-.03}$
Cn 3-1	$.487 \pm .005$	$3.69^{+.02}_{-.02}$						
H 1-35	$.378 \pm .017$	$4.37^{+.32}_{-.18}$	$0.483 \pm .033$	$4.29^{+1.6}_{-.29}$	$0.429 \pm .074$	$4.20^{+.17}_{-.19}$	$1.302 \pm .256$	$2.67^{+.63}_{-2.7}$
H 1-36			$0.503 \pm .023$	$4.09^{+.21}_{-.16}$	$0.397 \pm .039$	$4.28^{+.11}_{-.11}$	$0.253 \pm .008$	$4.74^{+.03}_{-.03}$
H 1-41			$0.813 \pm .040$	$3.12^{+.08}_{-.08}$	$1.101 \pm .150$	$3.12^{+.21}_{-.39}$	$1.214 \pm .063$	$3.01^{+.16}_{-.23}$
H 1-42			$0.532 \pm .014$	$3.91^{+.09}_{-.08}$	$0.719 \pm .093$	$3.69^{+.12}_{-.15}$	$0.704 \pm .020$	$3.88^{+.03}_{-.03}$
H 1-50	$.455 \pm .016$	$3.81^{+.08}_{-.07}$	$0.538 \pm .017$	$3.88^{+.09}_{-.08}$	$0.585 \pm .058$	$3.89^{+.09}_{-.11}$	$0.565 \pm .013$	$4.08^{+.02}_{-.02}$
H 1-54			$0.493 \pm .017$	$4.18^{+.18}_{-.14}$	$0.521 \pm .079$	$4.01^{+.14}_{-.16}$		
He 2-113	$.492 \pm .027$	$3.67^{+.10}_{-.09}$						
He 2-118	$.440 \pm .012$	$3.89^{+.06}_{-.06}$	$0.518 \pm .032$	$3.99^{+.24}_{-.18}$	$0.541 \pm .082$	$3.97^{+.14}_{-.16}$	$0.408 \pm .017$	$4.34^{+.03}_{-.03}$
He 2-136			$0.578 \pm .017$	$3.69^{+.06}_{-.06}$	$0.855 \pm .131$	$3.49^{+.17}_{-.24}$	$1.040 \pm .033$	$3.40^{+.05}_{-.06}$
He 2-142			$0.424 \pm .022$	$3.63^{+.00}_{-.00}$	$0.433 \pm .073$	$4.19^{+.17}_{-.19}$		
He 2-185			$0.617 \pm .030$	$3.56^{+.09}_{-.09}$	$0.893 \pm .080$	$3.44^{+.11}_{-.13}$	$0.781 \pm .024$	$3.78^{+.03}_{-.03}$
He 2-434			$0.571 \pm .078$	$3.71^{+.36}_{-.28}$	$1.000 \pm .150$	$3.29^{+.19}_{-.31}$	$0.926 \pm .026$	$3.58^{+.04}_{-.05}$
He 2-90			$0.439 \pm .042$	$3.44^{+.00}_{-.79}$	$0.752 \pm .130$	$3.64^{+.16}_{-.23}$		
He 2-97			$0.495 \pm .027$	$4.17^{+.34}_{-.22}$	$0.345 \pm .040$	$4.45^{+.15}_{-.14}$	$0.588 \pm .055$	$4.05^{+.08}_{-.09}$
He 3-1333	$.916 \pm .030$	$2.84^{+.05}_{-.05}$						
Hu 1-2	$.487 \pm .011$	$3.69^{+.04}_{-.04}$	$0.595 \pm .014$	$3.64^{+.05}_{-.05}$	$0.787 \pm .031$	$3.59^{+.05}_{-.05}$	$0.971 \pm .019$	$3.50^{+.03}_{-.03}$
Hu 2-1	$.424 \pm .006$	$3.97^{+.04}_{-.04}$						
IC 1297	$.570 \pm .022$	$3.45^{+.05}_{-.05}$	$0.645 \pm .021$	$3.48^{+.05}_{-.05}$	$0.943 \pm .071$	$3.36^{+.09}_{-.11}$	$1.009 \pm .021$	$3.44^{+.04}_{-.03}$
IC 3568	$.626 \pm .025$	$3.33^{+.05}_{-.05}$	$0.775 \pm .102$	$3.19^{+.19}_{-.22}$	$1.427 \pm .079$	$1.59^{+.83}_{-.00}$	$1.145 \pm .028$	$3.18^{+.06}_{-.06}$

Fig. 1. The observed [O II] $\lambda3729/\lambda3726$ ratio is plotted against the [S II] $\lambda6716/\lambda6731$ ratio for 37 nebulae. Triangles are H II regions from Tsamis et al. (2003) and Esteban et al. (2002). The dotted, solid and dashed lines delineate the theoretical variations of the [O II] ratio as a function of the [S II] ratio, assuming that both ions arise from identical ionization regions of uniform density, for an T_e of 5000 K, 10 000 K and 15 000 K, respectively. Along the lines, N_e increases from top right to bottom left, and the six filled circles denote densities of 10^0, 10^2, 10^3, 10^4, 10^5, 10^6 cm^{-3}, respectively. The dotted-dashed

Agreement for ions with similar I.P is encouraging, but it does appear that regions of different excitation may have different physical conditions.
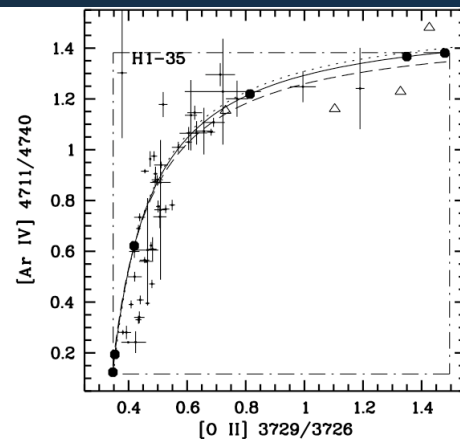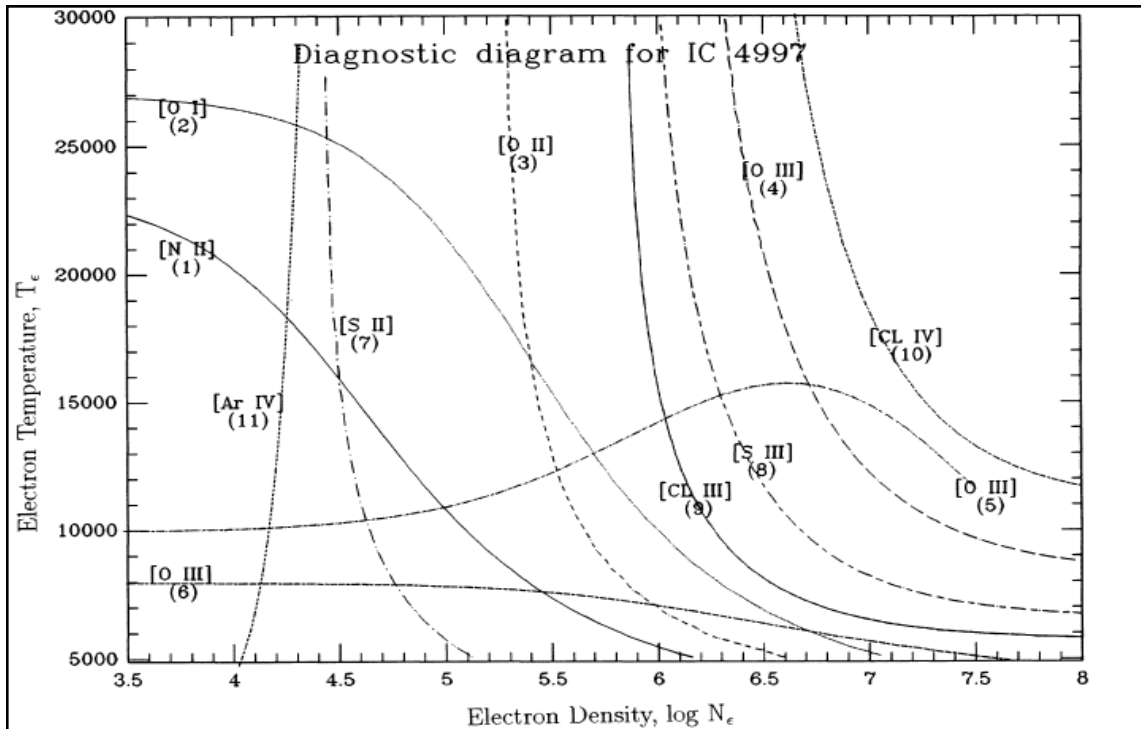

Fig. 4. Same as Fig. 1 but for [Ar IV] $\lambda4711/\lambda4740$ plotte [O II] $\lambda3729/\lambda3726$ for 36 nebulae.

The electron temperature- density diagnostic diagram for the young, dense planetary nebula IC 4997. using a range of collisionally excited lines. The fact that these curves do not intersect within a small area suggests that they rise from regions of different densities and temperatures (from Hyung et al 1994. ApJS 93, 465).

Other density indicators

High temperatures:
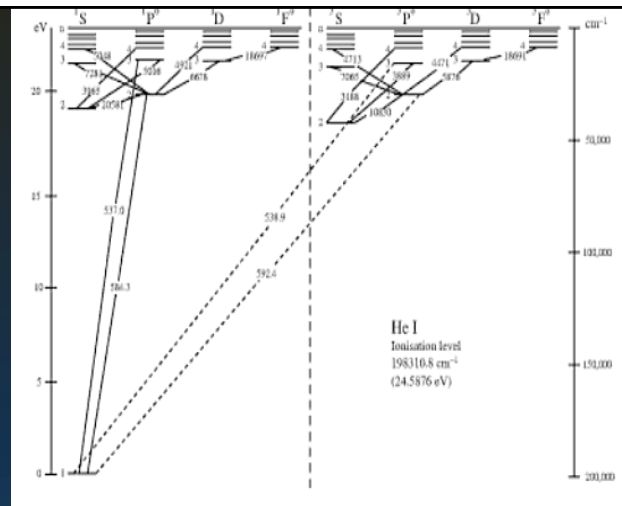
- He I- like ions: transitions in order of intensity:
- Permitted singlet line $1s^2\ {}^1S_0$ - $1s\ 2p\ {}^1P_1$.
- Forbidden line $1s^2\ {}^1S_0$ - $1s\ 2s\ {}^3S_1$ (breaks $\Delta L = 1$ selection rule).
- Intersystem line $1s^2\ {}^1S_0$ - $1s\ 2p\ {}^3P_1$ and $1s^2\ {}^1S_0$ - $1s\ 2p\ {}^3P_2$.

The 2nd and 3rd components are strongly forbidden and weak in He I, but the values increase substantially in He I like ions with large Z.
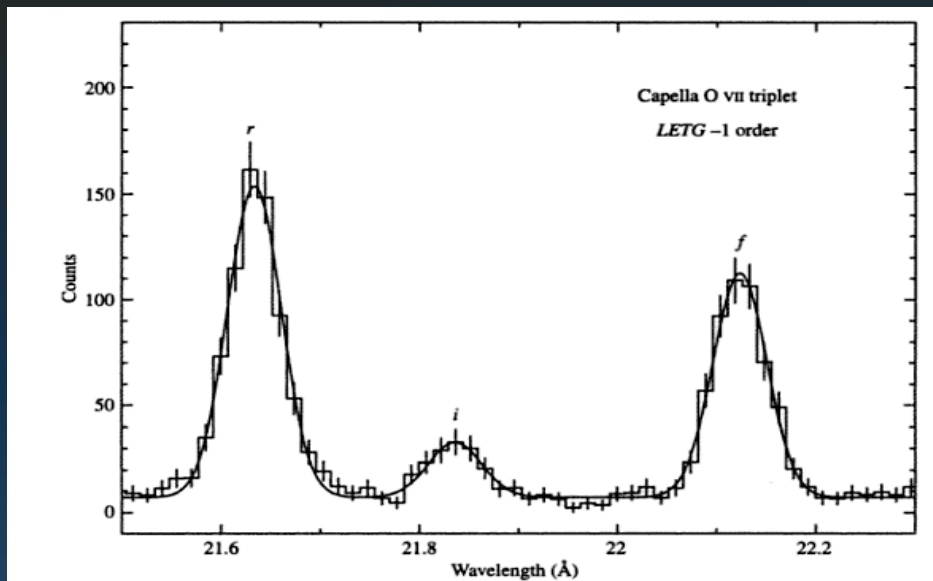
O VII in Capella

Figure 5.6
Chandra Low Energy Transmission Grating (LETG) spectrum of the star Capella showing the O VII $2^1P - 1^1S$ resonance line (labelled r), $2^3P - 1^1S$ intercombination line (labelled i), and the $2^3S - 1^1S$ forbidden line (labelled f). See the energy diagram of He for reference (Fig. 4.2). This triplet of lines is seen in many hot stars. (From Brinkman et al. 2000, ApJ, 530, L111.)

In O VII, the transitions are in the X–ray region, for which high quality spectra are available from Chandra and XMM-Newton.

At low densities, the 1s2s $^3S_1$ and 1s2p ^3P levels are populated by collisions from the ground state, and the ^3S level decays radiatively with probability A($^3S_1 - {}^1S_0$), but the $^3P_{1,2}$ levels can decay to both the ground state and the ^3S level. The $^3P_0$ level can only decay to the ^3S level as ΔJ=0 is not allowed when J=0.

At higher densities, collisional excitations from 1s2s ^3S to the 1s2p ^3P levels becomes increasingly important. These lead to higher intensity in the 1s2p $^3P_{1,2}$ - 1s^2 $^1S_0$ lines and lower intensity in the 1s2s $^3S_1$ - 1s^2 $^1S_0$ line.
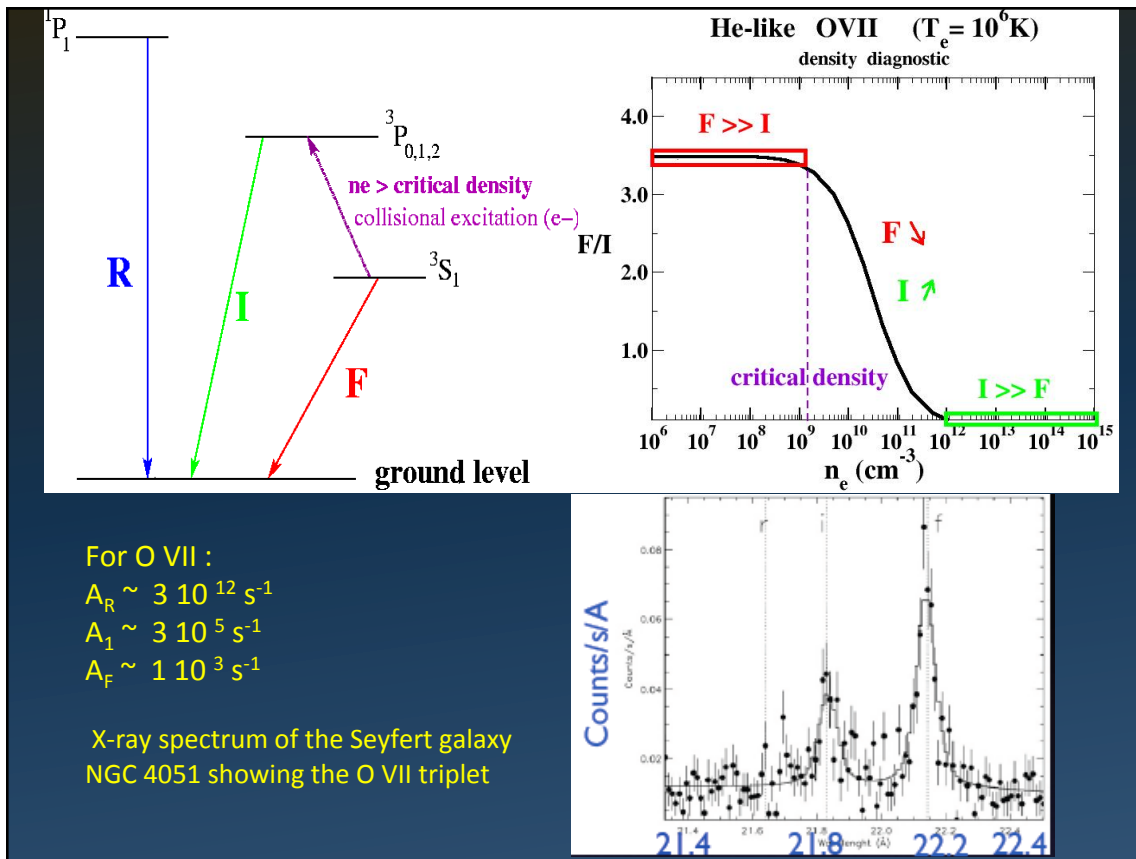
Here, the dependence upon N_e results from the competition between A($^3S_1 - {}^1S_0$) and the collisional excitation rate C($^3S_1 - {}^3P_{0,1,2}$)n_e.

The form of the expression is complicated, but these transitions provide diagnostics in the high density regime, with $n_e \sim 10^{16}$ m^{-3}.
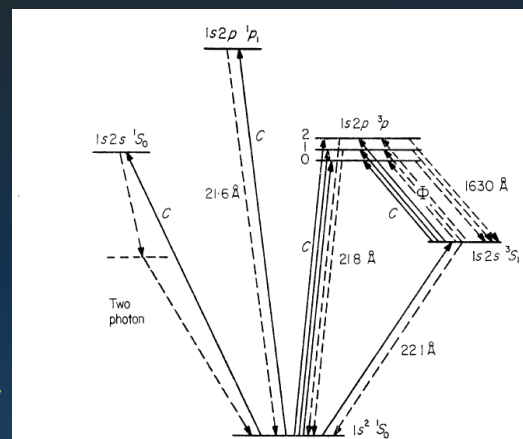
O VII Grotrian (energy level) diagram showing the transitions for the 21.6 Å Resonance, 21.8 Å Intercombination and 22.1 Å forbidden lines (from Gabriel & Jordan 1969).

He-like OVII $(T_e = 10^6 K)$
density diagnostic

For O VII :
$A_R \sim 3\ 10^{12}\ s^{-1}$
$A_1 \sim 3\ 10^5\ s^{-1}$
$A_F \sim 1\ 10^3\ s^{-1}$

X-ray spectrum of the Seyfert galaxy NGC 4051 showing the O VII triplet

Abundance estimates

- With good estimates for the n_e and T_e, the number of ions in a given level in a plasma can be determined from the measured line fluxes.
- With estimates of the level populations, and the distance, the ionic masses can be calculated.
- If all of the ionization states of an element are measured, the total element mass can be derived directly. Otherwise, the ionization structure of the nebula can be calculated by looking at the ratios of adjacent ions, and applying corrections based on a model ionization structure. (e.g. Cloudy developed by G Ferland at UKentucky)
- Because distance are often poorly determined, relative abundances are usually found by relating the element masses to the mass of H derived from recombination line or radio continuum measurements

- Overall there is good agreement using well-tested diagnostics, but some significant discrepancies remain. One area that is not fully understood is the discrepancy between element abundances for CNO found using forbidden and recombination lines. This may indicate a deficiency in nebula modelling or that HII regions are less homogenous in terms of T_e than expected.